HAL
open science

Thermal and structural modification in transparent and magnetic gallogermanate glasses induced by Gd2O3

Rayan Zaiter, Marc Dussauze, Marcelo Nalin, Evelyne Fargin, Frédéric Adamietz, Sylvain Danto, Olivier Toulemonde, Olivier Toulemonde, Thierry Cardinal

To cite this version:

Rayan Zaiter, Marc Dussauze, Marcelo Nalin, Evelyne Fargin, Frédéric Adamietz, et al.. Thermal and structural modification in transparent and magnetic gallogermanate glasses induced by Gd2O3. Journal of Alloys and Compounds, 2022, 912, pp.165181. 10.1016/j.jallcom.2022.165181 . hal-03870358

HAL Id: hal-03870358

https://hal.science/hal-03870358v1

Submitted on 25 Nov 2022

HAL is a multi-disciplinary open access archive for the deposit and dissemination of scientific research documents, whether they are published or not. The documents may come from teaching and research institutions in France or abroad, or from public or private research centers.

L'archive ouverte pluridisciplinaire **HAL**, est destinée au dépôt et à la diffusion de documents scientifiques de niveau recherche, publiés ou non, émanant des établissements d'enseignement et de recherche français ou étrangers, des laboratoires publics ou privés.

Thermal and structural modification in transparent and magnetic gallogermanate glasses induced by Gd_2O_3

Rayan Zaiter[a*], Marc Dussauze[b], Marcelo Nalin[c], Evelyne Fargin[a], Frédéric Adamietz[b], Sylvain Danto[a], Olivier Toulemonde[a], Thierry Cardinal[a]

[a] Institut de Chimie de la Matière Condensée de Bordeaux, Université de Bordeaux, 87 Avenue du Dr Schweitzer, Pessac F-33608, France

[b] Institut des Sciences Moléculaires, UMR 5255, Université de Bordeaux, 351 cours de la Libération, Talence Cedex 33405, France

[c] Institute of Chemistry – São Paulo State University-UNESP, Rua Prof. Francisco Degni, 55, CEP 14800-060, Araraquara - SP, Brazil

*Corresponding author: rayan.zaiter@icmcb.cnrs.fr

Abstract

A series of new transparent and magnetic barium gallogermanate glasses in the system (x) Gd_2O_3 – (100-x) [20BaO−15Ga_2O_3−65GeO_2] with x = 0, 8, 14, 18, 22 and 25 mol% were synthesized. Their thermal, structural and magnetic properties were characterized. Based on the differential scanning calorimetry results, one determined the composition domain exhibiting the highest thermal stability toward crystallization and provided a detailed experimental fabrication method for the production of optical fibers. The local glass structure investigated using combined Raman and Infrared vibrational spectroscopies shows a progressive depolymerization of the 3D glass germanate network accompanied with an increase of non-bridging oxygens when increasing the Gd_2O_3 content. The incorporation of gadolinium ions tends to extend the IR transmission window. Thanks to the magnetic susceptibility measurements, the paramagnetic behavior was evidenced, and increases with the Gd^{3+} content. The combination of the optical, thermal and magnetic properties of Gd_2O_3 gallogermanate glasses as well as their ability to be shaped into optical fibers make them promising materials for their integration in MIR functional optical components.

Keywords: magneto-optical materials, gallogermanate glasses, vibrational Raman and infrared spectroscopies, magnetic susceptibility

1. Introduction

Magneto-optical materials that can be used as magneto-optical current transducers or Faraday isolators are of interest for the development of mid-infrared (MIR) lasers, lab-on-chip photonic devices as well as in biological imaging and drug targeting [1]–[9]. While most of the research effort has been dedicated for the exploration of magneto-active materials for the visible and near-infrared (NIR) regions, the investigation on such materials transparent in the MIR domain are still very limited [4].

Although the magneto-optical phenomena seem to be more pronounced in crystals compared to glasses, the latter ones possess unique assets, among which their ability to be shaped into optical fibers. In the meantime, the synthesis of vitreous materials with high concentrations of rare earth oxides is challenging due to their tendency to devitrify during the cooling process [10], making it difficult to develop optical components. Besides, several glass systems possessing high concentrations of rare earth ions (even up to 37.5 mol% [11]) have been developed and reported in the literature such as germanates [12], [13], germanoborates [1], [2], [14], borates [15], aluminoborates [16], borosilicates [11], [17] aluminosilicates [18] and fluorophosphates [19]. However, none of these common oxide glass systems exhibits a transmission window extending from the ultraviolet region (UV) up to the MIR as the one represented by gallogermanate glasses. Such glasses also possess superior chemical, mechanical, and thermal resistance [20]. Among them, barium gallogermanate glass (so-called BGG), developed by the US Naval Research laboratory, were successfully employed as optical components either as low-loss optical fibers or bulk optical components [20]–[23]. Glass formation, structure, and properties of BGG glasses have been discussed earlier in the literature [20], [21], [24], [25].

In the present work, we report on the thermal, structural and magnetic evolution of a novel series of transparent glass in the system Gd_2O_3–BaO−Ga_2O_3−GeO_2. The characteristic temperatures and the glass thermal stability against crystallization were studied using Differential Scanning Calorimetry (DSC). The fiber drawing ability of these new glasses was also assessed. The glass structure was elucidated using the complementary vibrational spectroscopy techniques Raman and Infrared. Finally, the magnetic susceptibility measurements of the paramagnetic Gd^{3+} ions were characterized as a function of temperature.

2. Material and methods

2.1. Synthesis of glasses and preforms

Glasses were prepared by the traditional melt-quenching technique. The following raw materials : barium carbonate $BaCO_3$ (Fox Chemicals, 99.99%), gallium oxide Ga_2O_3 (Fox Chemicals, 99.999%), germanium oxide GeO_2 (Fox Chemicals, 99.999%) and gadolinium oxide Gd_2O_3 (Alfa Aesar, 99.999%) were weighed in the required proportions to prepare a series of batches of 7 grams. Then the

powders were mixed in a platinum crucible and heated up to 1550 °C for 1 to 2 h depending on the composition. The melted glasses were formed by quenching in ambient air. Glasses were then annealed at T_g − 40°C for 4 h and slowly cooled down to room temperature to reduce residual mechanical stress. All the resulting glasses were colorless, transparent and bubble free. Finally, glasses were cut and polished on both parallel faces for further characterizations.

Elaboration of the preforms for fiber drawing experiments was performed by melting and quenching 25 grams of glass into a stainless steel mold. Then preforms with dimensions of 1 cm in diameter and 7 cm in length were annealed (T_g − 40°C) and drawn following a protocol explained further below.

2.2. Physical and thermal characterizations

Characteristic temperatures which include the glass transition temperature (T_g), the onset of crystallization (T_x), and the maximum of the exothermic peak corresponding to the crystallization (T_C) were measured by differential scanning calorimetry using the Netzsch DSC Pegasus 404PC apparatus, on glass chunks in a Pt pan at a heating rate of 10 °C/min up to 1000 °C with a precision of ±2 °C. The thermal stability ($\Delta T = T_x - T_g$) was also calculated. The vitreous state of the samples studied was evaluated by XRD technique collected on a PANalitycal X'pert PRO MPD diffractometer in Bragg−Brentano θ−θ geometry equipped with a secondary monochromator and X'Celerator multi-strip detector. Each measurement was made within an angular range of 2θ = 8 − 80°. The Cu Kα radiation was generated at 45 kV and 40 mA (λ = 0.15418 nm).

The density, ρ, was obtained from the average of four measurements per sample using Archimedes' method by immerging a glass chunk in diethyl phthalate at room temperature on a Precisa XT 220A weighing scale with an estimated error of 0.005 g/cm^3.

The refractive index was determined by measuring the Brewster angle at 532 nm with an estimated error of ±0.005.

The transmission spectra in the UV-Visible-NIR and the IR ranges were respectively obtained from Agilent Cary 5000 (UV-Visible-NIR) and Bruker Equinox 55 (FTIR) spectrometers. The short wavelength cut-off (λ_{UV}) and the multiphonon cut-off (λ_{IR}) were determined from the recorded spectra for an absorption coefficient of 10 cm^{-1}.

2.3. Structural characterizations

Unpolarized Raman spectra were recorded with a confocal micro-Raman spectrometer LabRAM HR Evolution (Horiba Jobin Yvon) equipped with a Synapse CCD detector using a 532 nm radiation from a diode pumped solid state laser (output power = 20 mW). The incident laser beam was focused onto the sample through a microscope with a 10x objective (NA = 0.27, Olympus). Scattered light was dispersed by 1200 grooves/mm holographic grating system. Raman spectra have been corrected by the Bose-Einstein factor.

Reflectance infrared spectra have been recorded from 150 to 1500 cm^{-1} with a spectral resolution of 4 cm^{-1} using a Fourier Transform Spectrometer Vertex 70 V. A MIR source has been used (globar type). All measurements were performed in vacuum. The spectra have also been recorded from an average of 200 scans. Kramers-Kronig transforms have been performed in order to extract the real (n_0) and imaginary (k) parts of the refractive index n according to the relation $n = n_0 + ik$. Then the absorption coefficient was calculated using the relation $\alpha = 4\pi\nu k$, where ν is the frequency.

2.4. Magnetic susceptibility measurement

Magnetic susceptibility was collected using a Quantum Design MPMS-7XL magnetometer in the temperature range of 200 – 400 K under 1 T in a zero-field cooled mode.

3. Results and discussion

3.1. Physico-chemical properties

The investigated glass materials were selected in the system (x) Gd_2O_3 – (100-x) [$20BaO-15Ga_2O_3-65GeO_2$], with x = 0, 8, 14, 18 and 22 and 25 mol%. Their acronyms, nominal compositions in molar and cationic percent are summarized in Table 1. Fig. 1a shows a photograph of the synthesized glasses in this work. The samples with 0 up to 25 mol% of Gd_2O_3 are well transparent, colorless, homogeneous and chemically stable. Moreover, after synthesis, the glassy state was confirmed by the X-ray diffraction technique (results not shown). Fig. 1b shows the attraction of the sample with 22 mol% of Gd_2O_3 to a magnet. The same behavior was observed for all the other samples. However, based only on qualitative (visual) inspection at this stage, one should note that the magnetic force associated with the samples appears to be dependent on the concentration of paramagnetic ions as confirmed later below by the magnetic measurements.

Fig. 1. a) A photograph of glasses from 0 up to 25 mol% of Gd_2O_3 after cutting and polishing; b) sample with 25 mol% of Gd_2O_3 attracted by the magnet.

Table 1. Investigated glasses (acronyms, nominal compositions in molar and cationic percent) and their theoretical cationic ratios, i.e. $(3GdO_{3/2} + 2BaO)/GaO_{3/2}$.

	Nominal compositions (mol %)				**Nominal compositions (cat mol %)**				**Cationic ratios (cat mol %)**
Sample name	**Gd_2O_3**	**BaO**	**Ga_2O_3**	**GeO_2**	**$GdO_{3/2}$**	**BaO**	**$GaO_{3/2}$**	**GeO_2**	$Q = (3GdO_{3/2} + 2BaO) / GaO_{3/2}$
$0Gd_2O_3$	-	20	15	65	-	17.4	26.1	56.5	1.33
$8Gd_2O_3$	8.0	18.4	13.8	59.8	13.1	15.1	22.7	49.1	3.06
$14Gd_2O_3$	14.0	17.2	12.9	55.9	22.1	13.6	20.3	44.1	4.61
$18Gd_2O_3$	18.0	16.4	12.3	53.3	27.6	12.6	18.9	40.9	5.71
$22Gd_2O_3$	22.0	15.6	11.7	50.7	32.9	11.7	17.5	37.9	6.98
$25Gd_2O_3$	25.0	15	11.3	48.8	36.7	11.0	16.5	35.8	8.00

The glass transition temperature (T_g), onset of the crystallization event (T_x) and the crystallization peak (T_C) for each composition were determined by DSC and are summarized in Table 2. Fig. 2 shows the evolution of T_g and ΔT as a function of Gd_2O_3 concentration. The introduction of Gd_2O_3 is characterized by a linear increase of T_g from 668 °C for $0Gd_2O_3$ to 815 °C for $25Gd_2O_3$. Therefore, the presence of Gd_2O_3 in the glass increases the average strength of the chemical bonds. Later in the paper, based on the Raman and IR spectroscopy techniques, the structural evolution is described to better understand the connectivity evolution of these systems versus the amount of Gd_2O_3 introduced. For the $0Gd_2O_3$ sample, a crystallization peak appears around 794 °C. With the introduction of 8 mol% of Gd_2O_3, the peak shifts to 882 °C. For samples with concentrations greater than 8 mol% of Gd_2O_3, a secondary crystallization peak appears indicating the crystallization of different phases.

Table 2. Thermal and physical properties of the investigated glass samples (T_g: glass transition temperature, T_x: onset of the crystallization temperature T_C: crystallization temperature and ΔT: thermal stability criterion ($T_x - T_g$)) (ρ: density, λ_{UV}: short wavelength cut-off, λ_{IR}: multiphonon cut-off and n_{532nm}: refractive index at 532 nm).

Sample name	**T_g (±3 °C)**	**T_x (±3 °C)**	**T_{C1} (±3 °C)**	**T_{C2} (±3 °C)**	**ΔT (±4 °C)**	**ρ ($g.cm^{-3}$)**	**λ_{IR} (nm)**	**λ_{UV} (nm)**	**n_{532nm} (±0.005)**
$0Gd_2O_3$	668	776	794	-	108	4.568	5810	332	1.715
$8Gd_2O_3$	719	857	882	-	138	5.169	5840	316	1.810
$14Gd_2O_3$	752	872	904	925	120	5.566	5860	314	1.847
$18Gd_2O_3$	775	892	923	938	117	5.793	5900	308	1.841
$22Gd_2O_3$	802	910	933	958	108	6.023	5950	284	1.858
$25Gd_2O_3$	815	891	910	943	76	6.156	6000	284	1.867

The difference ΔT between the two characteristic temperatures T_g and T_x is often considered as a reliable criterion for evaluating the thermal stability *vs* crystallization of a glass. It makes it important in particular for its shaping by thermal process like glass fiber drawing (with targeted values of $\Delta T \geq$ 100 °C). One should note that the $8Gd_2O_3$ glass sample shows the highest thermal stability against crystallization with a value around 138 °C, which progressively decreased when increasing concentration of Gd_2O_3, to attain 76 °C for the $25Gd_2O_3$ glass.

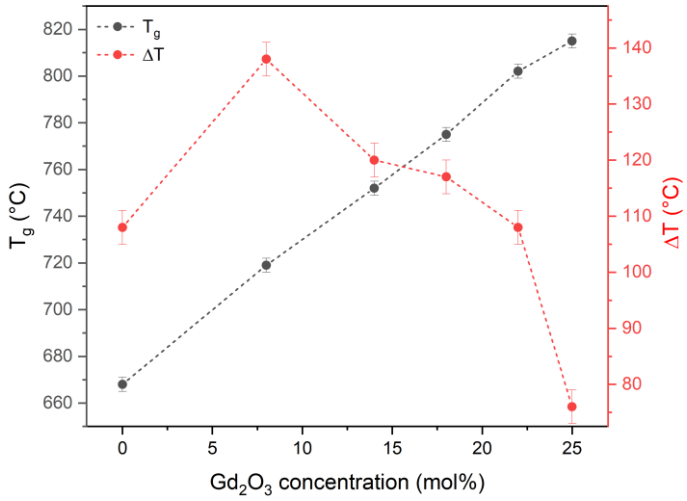

Fig. 2. The glass transition temperature (left) and the glass stability parameter against crystallization (right) as a function of the Gd_2O_3 concentration.

The measured density of the glasses is given in Table 2. Likewise the T_g evolution, density increases linearly with the addition of Gd_2O_3 from 4.568 g.cm^{-3} up to 6.156 g.cm^{-3} between the $0Gd_2O_3$ and $25Gd_2O_3$ samples respectively. This result can be readily explained by a higher density of the Gd_2O_3 component (7.407 g.cm^{-3}) compared to the other constituents of the glass. One can also note that the refractive index increases with increasing the Gd_2O_3 content, from 1.715±0.005 ($0Gd_2O_3$) to 1.867±0.005 ($25Gd_2O_3$).

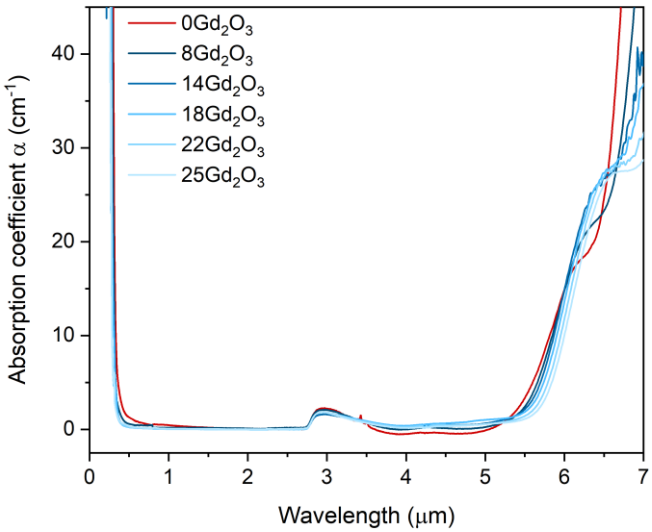

Fig. 3. Absorption coefficient of the glasses in the Gd_2O_3-containing gallogermanate glasses.

The absorption coefficient spectra of the gadolinium-containing gallogermanate glasses are displayed in Fig. 3. Spectra have been corrected for Fresnel reflections. A large transmission window is observed from the UV up to ~5500 nm for all the samples. The cut-off wavelengths have been determined for a given linear absorption coefficient of 10 cm^{-1} in the UV and the MIR.

Regarding the infrared multiphonon cut-off, the insertion of gadolinium in the glasses leads to an extending of the transparency window from 5810 nm ($0Gd_2O_3$) to 6000 nm ($25Gd_2O_3$). The infrared cut-off is dependent on the presence of an absorption band around 6.2 µm observed as a shoulder and the multi-phonon edge above 6.5 µm. The shift to the IR while increasing the Gd_2O_3 content corresponds to a shift toward high wavelengths of both the multi-phonon edge and the 6.2 µm absorption feature. Regarding the short wavelength cut-off, as shown in Fig. 3 and from the values presented in Table 2, one observe a small decrease from 332 ($0Gd_2O_3$) to 284 nm ($25Gd_2O_3$) with increasing the gadolinium concentration. This is expected because Gd_2O_3 has the largest band gap compared to all the other oxides used. One can notice an absorption band around 3 µm and a weak one around 4.2 µm related to the presence of OH groups in the glasses [26]. These absorption features are related to the absence of dehydration steps during the glass synthesis, similarly to previous observations made in tellurites [27].

3.2. Fabrication of magneto-optical glass fiber

One now turn our effort to produce optical fibers by the standard preform-to-fiber method. Owing to its highest thermal stability parameter against devitrification, two macroscopic mono-index glass preforms were selected for drawing, the $8Gd_2O_3$ (ΔT = 138 °C) and the $14Gd_2O_3$ (ΔT = 120 °C). Preform with the highest amount of gadolinium (14 mol% of Gd_2O_3) is shown in Fig. 4a.

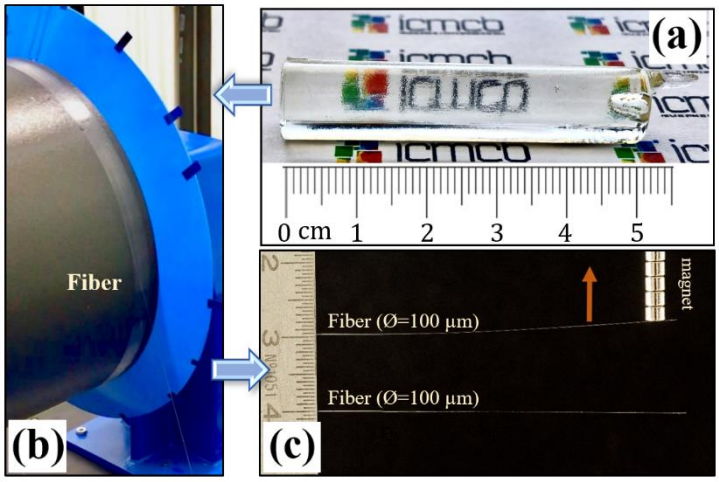

Fig. 4. Preform-based optical fiber manufacturing for $14Gd_2O_3$ glass (a) Photograph of macroscopic $14Gd_2O_3$ glass preform prior to drawing (b) glass fiber on drum and (c) fiber attracted to a Nd magnet.

The preforms were drawn using a dedicated optical fiber drawing towers equipped with an annular resistive furnace having a sharp temperature profile. The heating chamber was kept under continuous oxygen gas flow (3 $L.min^{-1}$). Preforms were fed into the furnace and the temperature was gradually increased up to ~600 °C using a heating rate of 20 °C/min, then to ~920 °C for $8Gd_2O_3$ and ~950 °C for $14Gd_2O_3$ with a heating rate of 10 °C/min to soften the bottom-sections of the preforms. Following this procedure, ~20-meter long fibers with diameters ranging from ϕ = 200 µm down to 100 µm (Fig. 4b) were fabricated.

Shaping gallogermanates into fibers is a difficult task due to the formation of zeolite crystal phase at temperatures above the glass transition temperature [22]. We have shown a proof of concept regarding this system because gadolinium addition allows to improve the thermal stability towards crystallization which is in agreement with findings of reference [28] stating that introduction of rare earth ions in germanogallate systems can contribute in mitigating the detrimental glass surface crystallization. In addition, it induces new magnetic properties as will be detailed below.

In order to qualitatively demonstrate the magnetic behavior of the $14Gd_2O_3$ glass fiber, one approach a neodymium magnet in its vicinity (Fig. 4c). It shows a small deviation of the fiber due to the magnetic attraction of the magnet. While magnetic property of the mono-index fiber is highlighted, the optical losses recorded at this stage (in the range 10-20 dB/m at 1 µm) remain too high for practical use. Such losses relate to the high viscosity of the melt, which leads to strong density fluctuation within the preform. Work is currently in progress to improve the preforms optical homogeneity, involving both the optimization of the glass composition and of the elaboration protocol.

3.3. Vibrational spectroscopy

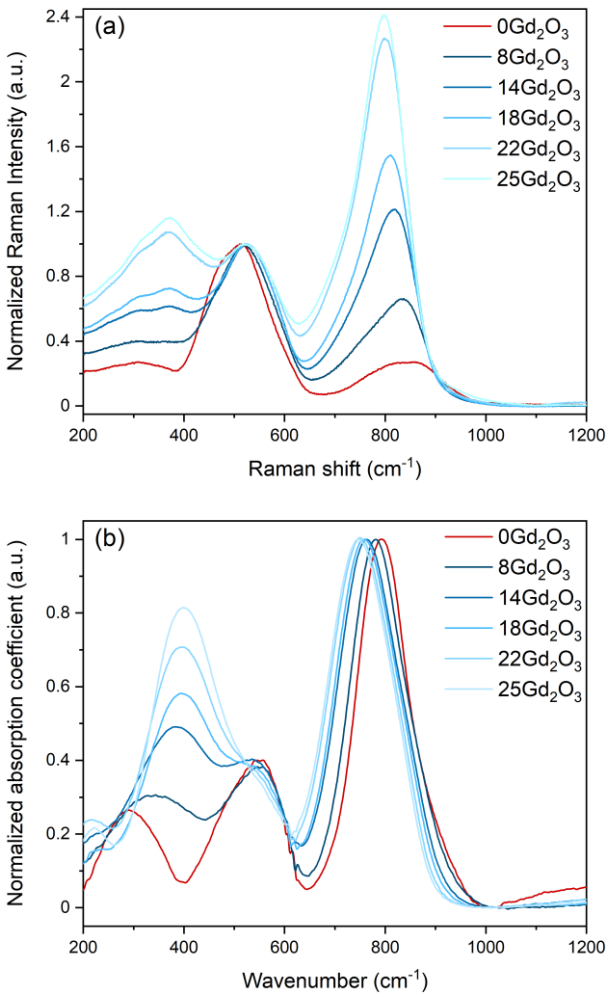

Fig. 5. Normalized (a) Raman and (b) Infrared spectra of samples with Gd_2O_3 concentrations from 0 to 25 mol%.

Unpolarized Raman and Infrared spectra for the investigated glass series are presented in Fig. 5. First, we focused on the vibrational spectra of the gallogermante matrix ($0Gd_20_3$) which can be decomposed into low (200 – 400 cm^{-1}), intermediate (400 – 640 cm^{-1}) and high frequency regions (640 − 1000 cm^{-1}). In the high-frequency region, vibrations can be assigned to stretching features of tetrahedral units of germanium or gallium [29]. The low and intermediate frequency envelopes can be attributed mainly to highly coupled bending δ ($T^{[4]}$ – O – $T^{[4]}$) modes of an oxygen surrounded by two corner-sharing tetrahedral units with T being either gallium or germanium; the brackets refer to the coordination number of the atoms [29]–[31]. One should remind that for the stretching (high frequency) spectral domain, the IR modes are always active. However, in Raman they are almost inactive for a GeO_2 glass and they are observable with a non-uniform charge distribution on the oxygen anions of the glass network by two reasons: (1) with mixed gallogermanate glass matrices, and the formation of $Ga^{[4]}$ – O^- – $Ge^{[4]}$ bridges [29] or (2) by the presence of non-bridging oxygens [32], [33]. In our case, for the gallogermanate matrix ($0Gd_20_3$), we have calculated $Q = [2BaO + 3GdO_{3/2}] / [GaO_{3/2}] > 1$ as can been seen in Table 1, thus we expect to see both latter modes.

To observe the evolutions with the Gd_2O_3 content, we normalized the Raman spectra to the band centered at 515 cm^{-1} because it is linked to the 3D network of germanium and gallium [24], and importantly it does not change too much in shape and position (~9 cm^{-1}) with the increase of Gd_2O_3 content. However, for the IR spectra, this band is located at 550 cm^{-1} and shifts down to ~530 cm^{-1} for 25 mol% of Gd_2O_3, as well as it merges with the low frequency bands. That is why it was easier to normalize the IR spectra to the most intense broad symmetrical band located around 790 cm^{-1}.

In the low frequency domain, a broad band rises in the same range (360-390 cm^{-1}) in both Raman and IR, and which increases with the Gd_2O_3 concentration. It can be related to the vibration of the Gd – O – Gd bonds attributed in cubic Gd_2O_3 as the F_g mode [34], [35]. The high-frequency region increases largely in intensity with the addition of gadolinium in Raman, and shifts from 793 cm^{-1} to 748 cm^{-1} with the disappearance of the right tail band in IR. This proves that the germanate network is affected either by the content of NBOs or the nature of charge compensation of these NBOs. This evolution can be compared to the red shift observed in the absorption spectra in Fig. 3. One can propose that the band observed around 6.2 µm corresponds to first overtone of the IR main mode around 800 cm^{-1}.

In order to enable a clear visualization of the spectral evolution of the gallogermanate network in the high-frequency region, deconvolution of the Raman spectra were conducted between the 600 − 1000 cm^{-1} range as shown in Fig. 6a-f. We have used the model from reference [31] for deconvolution because it works well with five Gaussian peak functions: at ~690 cm^{-1} (mode 1), ~758 cm^{-1} (mode 2), ~785 cm^{-1} (mode 3), ~838 cm^{-1} (mode 4) and ~890 cm^{-1} (mode 5). The variation of the peak position was maintained within ~5% while the width was kept fixed. The intermediate frequency region has been also fitted with a single Gaussian to enable a proper fitting of the high ones. The vibrational band assignments are presented in Table 3. According to the literature [33], modes 2 and 4 can be assigned to NBO on germanium tetrahedral moieties, respectively to Q^2 $(Ge\varnothing_2O_2)^{2-}$ and Q^3 $(Ge\varnothing_3O)^-$. Raman modes 3 and 5 can be attributed to localized asymmetric stretching vibrational modes involved in $Ge^{[4]} – O^- – Ga^{[4]}$ bridges [29]. The band at 700 cm^{-1} was necessary for the deconvolution and its origin will be discussed later. The key points observed in the structural evolution of the different entities are that Q^2 $(Ge\varnothing_2O_2)^{2-}$ and Q^3 $(Ge\varnothing_3O)^-$ increase largely and become the dominant ones with the addition of gadolinium, while the $Ge – O^- – Ga$ species are quite stable as shown in Fig. 6g. This model works well if taking into account the shift of the mode # 4, which shifts from ~854 cm^{-1} to ~810 cm^{-1}. This ~44 cm^{-1} shift is in accordance with the shift observed in IR. We can explain it by the change of the charge compensation of the NBOs. The 700 cm^{-1} band increases in the same manner as the NBO units, so it is certainly related to structural entities which are negatively charged, but at this stage we are not sure to distinguish between its attribution to modes in gallate units [36] or change in germanate or gallate coordination number [32], [33]. Complementary structural studies need to be performed by nuclear magnetic resonance (NMR) spectroscopy for instance, to have more detailed vibrational band assignments especially regarding the origin of the vibration around 700 cm^{-1}.

Table 3. Raman band assignments of the high frequency region in the Gd_2O_3–BaO−Ga_2O_3−GeO_2 glasses.

Band number	ν (cm^{-1})	Band assignments	Ref
1	700	GaO_n or GeO_n related vibrations	[32], [37]
2	760	ν (Ge – O) stretching of Q^2 $[GeØ_2O_2]^{2-}$ units	[32]
3	785	ν ($T^{[4]}$ – O – $T^{[4]}$) with Ga – O^- – Ge alternation	[29]
4	825	ν (Ge – O) stretching of Q^3 $[GeØ_3O]^-$ units	[32]
5	890	ν ($T^{[4]}$ – O – $T^{[4]}$) with Ga – O^- – Ge alternation	[30]

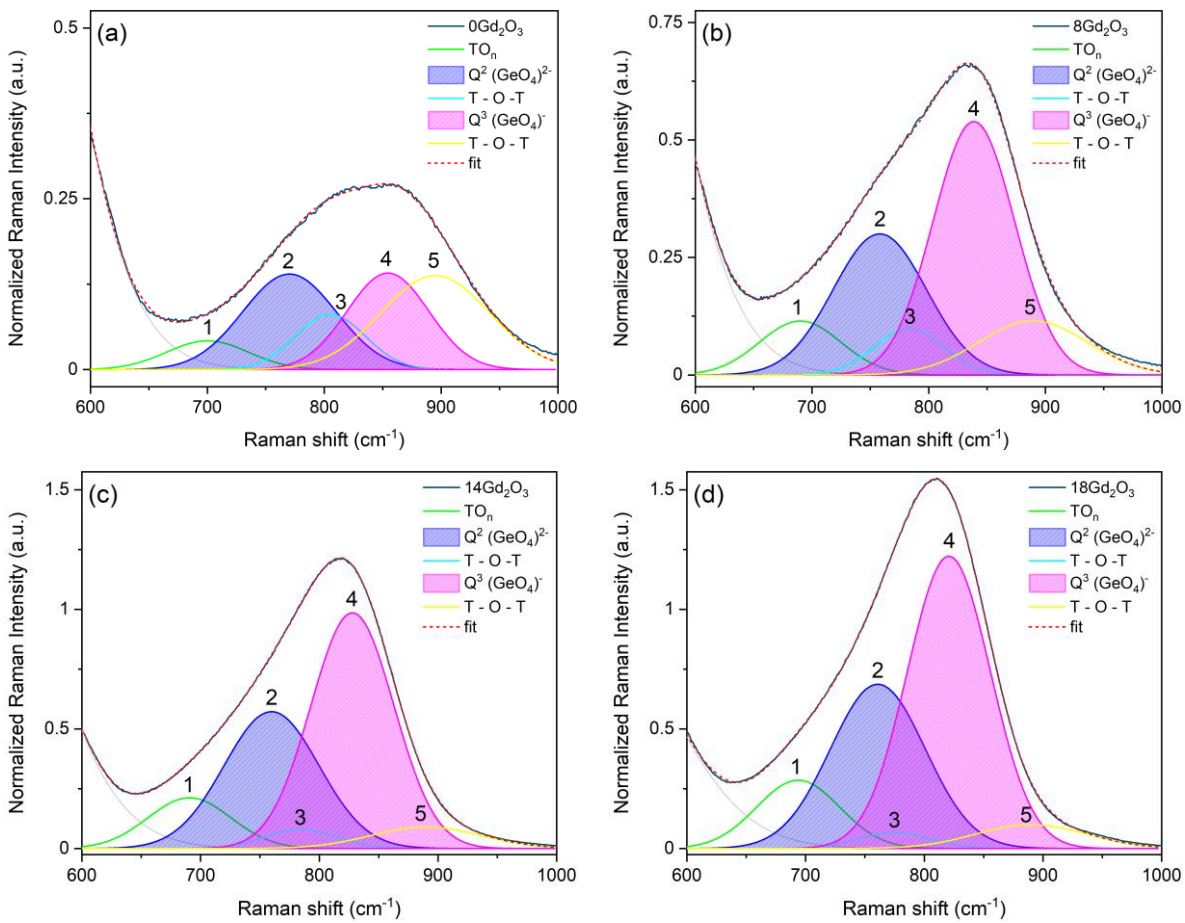

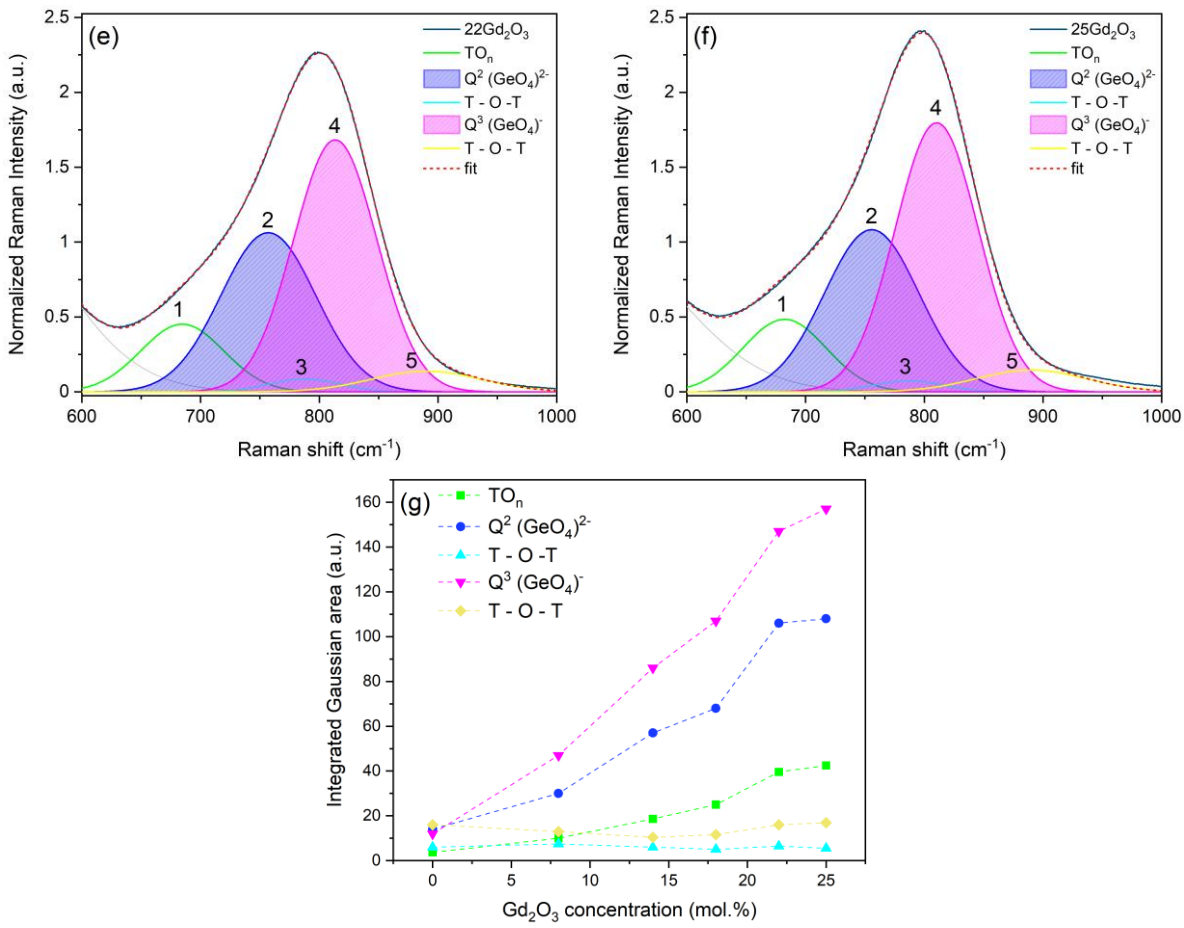

Fig. 6. Raman spectra deconvolutions with an error of ±5%: (a) $0Gd_2O_3$, (b) $8Gd_2O_3$, (c) $14Gd_2O_3$, (d) $18Gd_2O_3$, (e) $22Gd_2O_3$, (f) $25Gd_2O_3$. (g) The integrated Gaussian area of the modes TO_n, Q^2 $(GeO_4)^{2-}$, T – O – T, Q^3 $(GeO_4)^-$ and T – O – T as a function of the Gd_2O_3 concentration for a normalization at the 515 cm^{-1} band.

3.4. Magnetic properties

In order to study the magnetic behavior of the samples and to quantify the Gd_2O_3 content with respect to the targeted concentration, a magnetic susceptibility study was carried out over the temperature range 220 – 400 K. Fig. 7(a) shows the temperature dependence of magnetic susceptibilities for all glasses. When the temperature tends to zero, a paramagnetic behavior with an asymptotic trend is expected. In the inset of Fig. 7(a) is shown the inverse of susceptibility (1/χ) versus temperature. All the data were fitted according to the Curie-Weiss law, $\chi = \frac{C}{T-\theta}$, which allows to estimate the Curie constant (C) from the slope and the paramagnetic Curie temperature from the intercept. The values together with the coefficient of determination (R^2) to describe the quality of the fit are presented in Table 4. Even if positive and high values of θ would suggest the occurrence of ferromagnetic interactions between the rare earth ions, we believe that these high values are overestimated due to the temperature range that was considered during the data collection.

For x cationic mol% of $GdO_{3/2}$, one expects a targeted Gd^{3+} ion content of $2x$ cationic mol%. Fig. 7(b) shows that our analysis presents a good agreement between the targeted and the probed Gd^{3+} ion concentrations. The deviation of the highest probed concentration (41.93 cationic mol% of $GdO_{3/2}$) from linearity might be probably due to GeO_2 evaporation from the melt because of the very high temperature of the synthesis (~1550 °C) which could lead to germanium oxide loss and then over estimation of the gadolinium content.

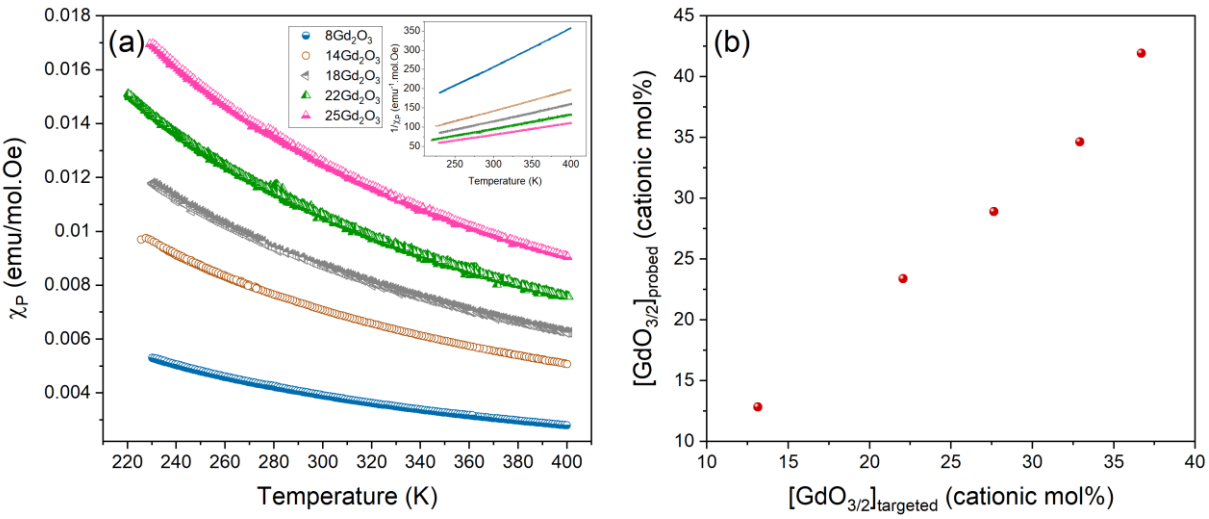

Fig. 7. (a) Magnetic molar susceptibility (χ_m) vs temperature measurements for a series of glasses according to the Gd_2O_3 concentration. The inset shows the $1/\chi$ vs T plot demonstrating the validity of the Curie-Weiss law in the temperature range 220 – 400 K. (b) Plot of the targeted Gd^{3+} content versus the probed one (error bars are plotted ranging from ± 0.01 to ± 0.05, however they are masked by the size of the red dots).

Table 4. Parameters obtained from the Curie-Weiss fits of the magnetic susceptibility data for all the studied glasses, where C is the Curie constant, θ is the Weiss temperature, χ_{diam} is the diamagnetic susceptibility and R^2 is the coefficient of determination.

mol% of Gd_2O_3	**C (emu.K/mol)**	**θ (K)**	**χ_{diam}(*10^{-5} emu/mol)** [38]	**R^2**
8%	1.011 ± 0.001	40.64 ± 0.29	-1.69	0.99961
14%	1.841 ± 0.001	39.11 ± 0.22	-1.86	0.99981
18%	2.275 ± 0.003	38.15 ± 0.39	-1.98	0.99938
22%	2.728 ± 0.003	41.06 ± 0.31	-2.09	0.99884
25%	3.302 ± 0.004	35.93 ± 0.36	-2.18	0.99944

The results ascertain the paramagnetic behavior of the Gd^{3+} ions, which were expected to be well-dispersed throughout the glass matrix. As can be seen in Figure 1, the glass is attracted by a magnet.

Such observation supports the fact that Gd^{3+} ions can align themselves along the magnetic field. Once the magnetic field is not present anymore, no magnetic behavior is observed.

Based on their unique magnetic properties, but also on their extended optical transmission and the successful demonstration of their drawing into fibers, one considered the newly developed Gd_2O_3-containing glasses exposed here as materials of interest for further effective integration into MIR functional optical components.

4. Conclusions

The introduction of high loading of Gd^{3+} ions in barium gallogermanate glass matrix provides a paramagnetic character of the materials. In the glass system Gd_2O_3−BaO−Ga_2O_3−GeO_2 in which up to 25 mol% of Gd_2O_3 have been hosted, we have clearly confirmed that the Gd^{3+} ions are the only paramagnetic species. Raman and infrared analysis showed that the Gd_2O_3 incorporation in the gallogermanate glass matrix induced depolymerization of the tetrahedral germanium oxide network forming non-bridging oxygens on the germanate moieties. Besides exhibiting good optical properties such as a transparency window up to 5.5 µm, glasses up to 18 mol% of Gd_2O_3 content showed a good thermal stability against crystallization with T_x-T_g above 100 °C. This merit combined with their magnetic behavior make such glasses promising materials for the manufacture of optical fibers which has been effectively demonstrated.

Acknowledgements

This research was supported by Agence Nationale de la Recherche (ANR) (ANR Grant ANR-18-CE08-0004-02), the CPER Campus B, and the New Aquitaine region (Grant 2016-1R10107). M. Nalin acknowledge the São Paulo Research foundation FAPESP (grant numbers 2013/07793-6 and 2019/01223-0). This project has received funding from the European Union's Horizon 2020 research and innovation program under the Marie-Skłodowska-Curie grant agreement N°823941 (FUNGLASS).

References

[1] R. G. Fernandes, D. F. Franco, V. R. Mastelaro, T. Cardinal, O. Toulemonde, and M. Nalin, "Thermal and structural modification in transparent and magnetic germanoborate glasses induced by Gd_2O_3," *Ceramics International*, vol. 46, no. 14, pp. 22079–22089, Oct. 2020, doi: 10.1016/j.ceramint.2020.05.227.

[2] D. F. Franco *et al.*, "Magneto-optical borogermanate glasses and fibers containing Tb^{3+}," *Sci Rep*, vol. 11, p. 9906, May 2021, doi: 10.1038/s41598-021-89375-1.

[3] Z. X. Mo, H. W. Guo, P. Liu, Y. D. Shen, and D. N. Gao, "Luminescence properties of magneto-optical glasses containing Tb^{3+} ions," *Journal of Alloys and Compounds*, vol. 658, pp. 967–972, Feb. 2016, doi: 10.1016/j.jallcom.2015.10.236.

[4] D. Vojna, O. Slezák, A. Lucianetti, and T. Mocek, "Verdet Constant of Magneto-Active Materials Developed for High-Power Faraday Devices," *Applied Sciences*, vol. 9, no. 15, Art. no. 15, Jan. 2019, doi: 10.3390/app9153160.

[5] D. Vojna, O. Slezák, R. Yasuhara, H. Furuse, A. Lucianetti, and T. Mocek, "Faraday Rotation of Dy_2O_3, CeF_3 and $Y_3Fe_5O_{12}$ at the Mid-Infrared Wavelengths," *Materials (Basel)*, vol. 13, no. 23, p. 5324, Nov. 2020, doi: 10.3390/ma13235324.

[6] D. F. Franco *et al.*, "Fundamental studies of magneto-optical borogermanate glasses and derived optical fibers containing Tb^{3+}," *Journal of Materials Research and Technology*, vol. 11, pp. 312–327, Mar. 2021, doi: 10.1016/j.jmrt.2021.01.010.

[7] C. Xu, M. Ou, H. Zhou, and C. Yang, "Preparation and properties of bifunctional Gd_2O_3/GQD composite nanoparticles," *Journal of Rare Earths*, Jul. 2021, doi: 10.1016/j.jre.2021.06.010.

[8] P. Zu *et al.*, "Magneto-optic fiber Sagnac modulator based on magnetic fluids," *Opt. Lett., OL*, vol. 36, no. 8, pp. 1425–1427, Apr. 2011, doi: 10.1364/OL.36.001425.

[9] J. Dai and J. Li, "Promising magneto-optical ceramics for high power Faraday isolators," *Scripta Materialia*, vol. 155, pp. 78–84, Oct. 2018, doi: 10.1016/j.scriptamat.2018.06.031.

[10] M. Kim, C. L. Corkhill, N. C. Hyatt, and J. Heo, "Development, characterization and dissolution behavior of calcium-aluminoborate glass wasteforms to immobilize rare-earth oxides," *Sci Rep*, vol. 8, no. 1, p. 5320, Mar. 2018, doi: 10.1038/s41598-018-23665-z.

[11] H. Luo, X. Hu, W. Liu, Y. Zhang, A. Lu, and X. Hao, "Compositional dependence of properties of Gd_2O_3–SiO_2–B_2O_3 glasses with high Gd_2O_3 concentration," *Journal of Non-Crystalline Solids*, vol. 389, pp. 86–92, Apr. 2014, doi: 10.1016/j.jnoncrysol.2014.02.017.

[12] M. R. Prakash *et al.*, "Holmium doped bismuth-germanate glasses for green lighting applications: A spectroscopic study," *Optical Materials*, vol. 94, pp. 436–443, Aug. 2019, doi: 10.1016/j.optmat.2019.05.003.

[13] L. Pop, M. Bosca, and E. Culea, "Spectroscopic and magnetic behavior of Gd and Nd ions in lead–germanate glasses," *Journal of Alloys and Compounds*, vol. 525, pp. 58–62, Jun. 2012, doi: 10.1016/j.jallcom.2012.02.069.

[14] X.-Y. Sun *et al.*, "Eu^{3+}-Activated Borogermanate Scintillating Glass with a High Gd_2O_3 Content," *Journal of the American Ceramic Society*, vol. 96, no. 5, pp. 1483–1489, 2013, doi: 10.1111/jace.12205.

[15] M. Zagrai, M. Unguresan, S. Rada, J. Zhang, M. Pica, and E. Culea, "Local structure in gadolinium-lead-borate glasses and glass-ceramics," *Journal of Non-Crystalline Solids*, vol. 546, p. 120259, Oct. 2020, doi: 10.1016/j.jnoncrysol.2020.120259.

[16] P. Lertloypanyachai *et al.*, "Luminescence, scintillation, and energy transfer in SiO_2–Al_2O_3–B_2O_3–Gd_2O_3:Ce^{3+},Pr^{3+} glasses," *physica status solidi (a)*, vol. 214, no. 9, p. 1700072, 2017, doi: 10.1002/pssa.201700072.

[17] J. Fu, J. M. Parker, R. M. Brown, and P. S. Flower, "Compositional dependence of scintillation yield of glasses with high Gd_2O_3 concentrations," *Journal of Non-Crystalline Solids*, vol. 326–327, pp. 335–338, Oct. 2003, doi: 10.1016/S0022-3093(03)00428-9.

[18] S. Ju *et al.*, "Temperature and Vibration Dependence of the Faraday Effect of Gd_2O_3 NPs-Doped Alumino-Silicate Glass Optical Fiber," *Sensors*, vol. 18, no. 4, Art. no. 4, Apr. 2018, doi: 10.3390/s18040988.

[19] B. Bellanger, Y. Ledemi, and Y. Messaddeq, "Fluorophosphate Glasses with High Terbium Content for Magneto-optical Applications," *J. Phys. Chem. C*, vol. 124, no. 9, pp. 5353–5362, Mar. 2020, doi: 10.1021/acs.jpcc.9b11696.

[20] S. S. Bayya, B. B. Harbison, J. S. Sanghera, and I. D. Aggarwal, "BaO-Ga_2O_3-GeO_2 glasses with enhanced properties," *Journal of Non-Crystalline Solids*, vol. 212, no. 2, pp. 198–207, Jun. 1997, doi: 10.1016/S0022-3093(96)00658-8.

[21] S. S. Bayya, G. D. Chin, J. S. Sanghera, and I. D. Aggarwal, "Germanate glass as a window for high energy laser systems," *Opt. Express, OE*, vol. 14, no. 24, pp. 11687–11693, Nov. 2006, doi: 10.1364/OE.14.011687.

[22] S. S. Bayya, J. S. Sanghera, I. D. Aggarwal, and J. A. Wojcik, "Infrared Transparent Germanate Glass-Ceramics," *Journal of the American Ceramic Society*, vol. 85, no. 12, pp. 3114–3116, 2002, doi: 10.1111/j.1151-2916.2002.tb00594.x.

[23] S. S. Bayya, J. S. Sanghera, and I. D. Aggarwal, "Optical transmission of BGG glass material," US7285509B2, Oct. 23, 2007 Accessed: Jul. 19, 2021. [Online]. Available: https://patents.google.com/patent/US7285509B2/en

[24] D. M. McKeown and C. I. Merzbacher, "Raman spectroscopic studies of BaO-Ga_2O_3-GeO_2 glasses," *Journal of Non-Crystalline Solids*, vol. 183, no. 1, pp. 61–72, Apr. 1995, doi: 10.1016/0022-3093(94)00648-2.

[25] C. Merzbacher, “Infrared reflectance of barium gallogermanate glasses,” *Physics and Chemistry of Glasses*, vol. 33, no. 6, pp. 233–238, 1992.

[26] J. M. Jewell and I. D. Aggarwal, “Structural influences on the hydroxyl spectra of barium gallogermanate glasses,” *Journal of Non-Crystalline Solids*, vol. 181, no. 1, pp. 189–199, 1995, doi: 10.1016/0022-3093(94)00471-4

[27] G. Guéry *et al.*, “Influence of Hydroxyl Group on IR Transparency of Tellurite- Based Glasses,” 2014, doi: 10.1111/IJAG.12044.

[28] T. Guérineau *et al.*, “Extended germano-gallate fiber drawing domain: from germanates to gallates optical fibers,” *Optical Materials Express*, vol. 9, p. 2437, Jun. 2019, doi: 10.1364/OME.9.002437.

[29] T. Skopak *et al.*, “Structure and Properties of Gallium-Rich Sodium Germano-Gallate Glasses,” *J. Phys. Chem. C*, vol. 123, no. 2, pp. 1370–1378, Jan. 2019, doi: 10.1021/acs.jpcc.8b08632.

[30] T. Skopak *et al.*, “Properties, structure and crystallization study of germano-gallate glasses in the Ga_2O_3-GeO_2-BaO-K_2O system,” *Journal of Non-Crystalline Solids*, vol. 514, pp. 98–107, Jun. 2019, doi: 10.1016/j.jnoncrysol.2019.02.028.

[31] F. Calzavara *et al.*, “Glass forming regions, structure and properties of lanthanum barium germanate and gallate glasses,” *Journal of Non-Crystalline Solids*, vol. 571, p. 121064, Nov. 2021, doi: 10.1016/j.jnoncrysol.2021.121064.

[32] E. I. Kamitsos, Y. D. Yiannopoulos, M. A. Karakassides, G. D. Chryssikos, and H. Jain, “Raman and Infrared Structural Investigation of $xRb_2O{\cdot}(1-x)GeO_2$ Glasses,” *J. Phys. Chem.*, vol. 100, no. 28, pp. 11755–11765, Jan. 1996, doi: 10.1021/jp960434+.

[33] G. S. Henderson, L. G. Soltay, and H. M. Wang, “Q speciation in alkali germanate glasses,” *Journal of Non-Crystalline Solids*, vol. 356, no. 44, pp. 2480–2485, Oct. 2010, doi: 10.1016/j.jnoncrysol.2010.03.023.

[34] C. L. Luyer, A. García-Murillo, E. Bernstein, and J. Mugnier, “Waveguide Raman spectroscopy of sol–gel Gd_2O_3 thin films,” *Journal of Raman Spectroscopy*, vol. 34, no. 3, pp. 234–239, 2003, doi: 10.1002/jrs.980.

[35] M. W. Urban and B. C. Cornilsen, “Bonding anomalies in the rare earth sesquioxides,” *Journal of Physics and Chemistry of Solids*, vol. 48, no. 5, pp. 475–479, Jan. 1987, doi: 10.1016/0022-3697(87)90108-9.

[36] K. Yoshimoto, A. Masuno, M. Ueda, H. Inoue, H. Yamamoto, and T. Kawashima, "Low phonon energies and wideband optical windows of La_2O_3-Ga_2O_3 glasses prepared using an aerodynamic levitation technique," *Sci Rep*, vol. 7, no. 1, pp. 1–9, Mar. 2017, doi: 10.1038/srep45600.

[37] S. Szu, C. Shu, and L.-G. Hwa, "Structure and properties of lanthanum galliogermanate glasses," *Journal of Non-Crystalline Solids*, vol. 240, no. 1, pp. 22–28, Oct. 1998, doi: 10.1016/S0022-3093(98)00710-8.

[38] G. A. Bain and J. F. Berry, "Diamagnetic Corrections and Pascal's Constants," *J. Chem. Educ.*, vol. 85, no. 4, p. 532, Apr. 2008, doi: 10.1021/ed085p532.